Title

Iodide Double Perovskites and the Limits of their Structural Stability

Journal

Chemistry — A European Journal, 31(8)

ISSN

0947-6539 1521-3765

Authors

Mulligan, Anya S

Kent, Greggory T

Zhuang, Jiale

et al.

Publication Date

2024-11-22

DOI

10.1002/chem.202404009

Peer reviewed

Iodide Double Perovskites and the Limits of their Structural Stability

Anya S. Mulligan,[+,a] Greggory T. Kent,[+,a] Jiale Zhuang,[a] Arava Zohar,[a]

Kaitlin R. Albanese,[a] Emily E. Morgan, [a] Guang Wu, [a] Anthony K. Cheetham, [c,*]

Ram Seshadri[a,b,*]

[a] Anya S. Mulligan, Dr. Greggory T. Kent, Jiale Zhuang, Dr. Kaitlin R. Albanese, Dr. Emily E. Morgan, Dr. Arava Zohar
Materials Department and Materials Research Laboratory
University of California, Santa Barbara, California 93106, United States

[b] Dr. Guang Wu
Department of Chemistry and Biochemistry
University of California, Santa Barbara, California 93106, United States

[c] Professor Sir Anthony K. Cheetham
Materials Department and Materials Research Laboratory
University of California, Santa Barbara, California 93106,
United States Department of Materials Science and Engineering
National University of Singapore, Singapore 117575,
Singapore
Email: akc30@cam.ac.uk

[c] Professor Ram Seshadri
Materials Department and Materials Research Laboratory Department of Chemistry and Biochemistry
University of California, Santa Barbara, California 93106,
United States
Email: seshadri@mrl.ucsb.edu

[+] These authors contributed equally.

Dedicated to Professor C. N. R. Rao FRS on the occasion of his 90th birthday.

Abstract

While halide double perovskites $A_2M(I)M(III)X_6$ have attracted significant attention, examples involving iodides are rare. We examine the limits of the structural stability of iodide double perovskites, presenting the synthesis and single-crystal structures of Cs_2NaScI_6 and Cs_2NaYI_6. Bypassing the common expectation that iodides have small band gaps, these compounds display optical gaps of 3.10 eV [M(III) = Sc] and 3.65 eV [M(III) = Y]. Cs_2NaScI_6 is the only iodide double perovskite to exhibit a cubic crystal structure at room temperature. Density functional theory-based electronic structure calculations help understand the role of competing $Cs_3M(III)_2I_9$ (3:2:9) phases and provide possible reasons for why iodide double perovskites based around In(III), Sb(III) and Bi(III) cations have proved elusive. We confirm design rules for halide double perovskite based around concepts of the tolerance factor and the radius ratio of the smaller, trivalent ion, but also point to situations such as what is observed for Cs_2NaScI_6 where a double perovskite can be trapped in a metastable structure.

Keywords: Halides • Double Perovskites • Iodides • Optical Properties • Stability

Introduction

Double perovskites are formed by the ordered arrangement of two different cations within the parent perovskite framework, allowing for a wide range of composition and function. These materials have long been recognized for their versatile crystal chemistry and their potential across numerous applications.[1] Interest in double perovskites has reignited after the emergence of hybrid lead halide perovskites as standout optoelectronic materials.[2, 3, 4, 5, 6, 7, 8] However, stability and toxicity challenges have prompted the exploration of lead-free alternatives, resulting in a huge expansion of the halide perovskite literature.[9, 10, 11, 12] Bismuth(III) naturally emerges as a promising candidate for retaining the sought-after properties of lead halide perovskites while mitigating the drawbacks.[13] Moving from the parent AMX_3 (A = large monovalent cation, M = smaller divalent cation, and X is halide) structure to the double perovskite $A_2M(I)M(III)X_6$ structure allows concurrent replacement of two Pb(II) ions with a Bi(III) and an M(I) ion. While attainable for the bromide-based double perovskites $A_2M(I)BiBr_6$, [14, 15, 16] the analogous all-inorganic iodide structure Cs_2AgBiI_6 was only recently isolated through anion exchange of $Cs_2AgBiBr_6$.[17] While much of the recent focus has been on hybrid organic-inorganic double perovskites, all-inorganic compositions featuring Cs on the A site generally have superior mechanical and thermal stability.[1,18]

Iodide double perovskites are of particular interest because they typically have narrower band gaps than the corresponding chlorides or bromides, potentially making them useful for

visible and near-IR optoelectronic applications.[19] Furthermore, the higher atomic number means that the iodides would have superior stopping power for use in radiation detection, which is another important application.[20,21] Unfortunately, few iodide double perovskites have been realized and the majority of these only recently.[22,17] In contrast to 3D variants, layered iodide double perovskites,[23, 24] are not uncommon, and the functionality of several have been established.[25, 26, 27] The formation of double perovskites is generally explained by the need to satisfy two geometric descriptors,[28] the double perovskite tolerance factor [29] t' and the radius ratio (cation radius:anion radius) μ— also called the octahedral factor.[30] Since the monovalent ion is usually large (Na^+ or Ag^+), the radius ratio is only a consideration for the trivalent ion *M*(III). These geometric constraints preclude many trivalent cations from an octahedral coordination environment with iodide. In addition, the formation of competing 3:2:9 iodide phases [31, 32, 33, 34] could explain the absence of some structures that are predicted based on μ and t'. While chlorides and bromides also form these 3:2:9 phases, they are particularly relevant to iodides, which is explained by the preference for large anions to favor lower-dimensional structures.[35]

Here we examine the stability range of iodide double perovskites in a more quantitative manner. We report the solid-state synthesis of two rare-earth iodide double perovskites following the general formula Cs_2NaMI_6 (*M* = Sc, Y). Solid state synthesis is preferred since solution methods do not yield the products obtained here, as described previously.[22] Reaction conditions for forming the Sc compound also yield the 3:2:9 composition, $Cs_3Sc_2I_9$, with discrete face-shared $Sc_2I_9^{3-}$ moieties, and a single crystal structure has been obtained. Cs_2NaScI_6 and $Cs_3Sc_2I_9$ have been previously reported [36,37] but with limited characterization. Optical absorption measurements carried out here suggest these iodide double perovskites have wide (> 3 eV) band gaps. Electronic structure calculations indicate that the Sc double perovskite is metastable and point to why iodide double perovskites with *M*(III) = In, Sb, and Bi have not been reported through direct synthesis.

Results and Discussion

The compounds were prepared by solid-state reaction followed by vapor transport in sealed and evacuated silica tubes, with all reactant and sample manipulation under strictly air-free and anhydrous conditions. Cs_2NaScI_6 was obtained as faint yellow powders and Cs_2NaYI_6 powders were almost white. The reaction conditions for Cs_2NaScI_6 often yielded $Cs_3Sc_2I_9$ crystals. Bulk powders of the latter could be readily prepared using the procedure detailed above, but with 2 equivalents ScI_3 and 3 equivalents CsI. More details are provided in the Supporting Information. To avoid issues with twinning of crystals, as found previously in the other iodide double perovskites,[22] structural studies were initially carried out at T = 414 K — a temperature where both compounds are cubic.

Figure 1 shows the structures of Cs_2NaScI_6 and Cs_2NaYI_6 at T = 414 K and at room temperature (T = 298 K). Single-crystal refinement confirms Cs_2NaScI_6 is the only known iodide with the cubic double perovskite structure at room temperature, and that this structure is retained at T = 414 K. This cubic structure has $Fm\bar{3}m$ space group symmetry and is analogous to the K_2NaAlF_6 elpasolite structure. At T = 414 K Cs_2NaYI_6 adopts this cubic double perovskite structure, which made complete structural determination possible. Cooling Cs_2NaYI_6 to room temperature resulted in a structural transition, but issues with twinning prevented robust structural refinement. However, the powder XRD Pawley fit showed that the room-temperature data for Cs_2NaYI_6 is most consistent with the monoclinic $P2_1/n$ space group. Pawley fits of powder XRD data for both double perovskite compounds are presented in the Supporting Information. Accurate room-temperature unit cell parameters of Cs_2NaYI_6 obtained from the Pawley fit at T = 298 K were employed to carry out density functional theory-based structure relaxations of the internal atomic structure. It is this structure that is depicted for Cs_2NaYI_6 at T = 298 K.

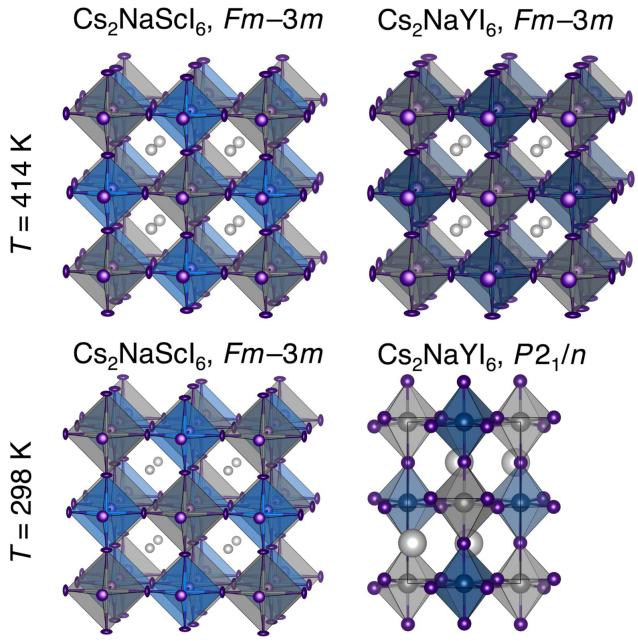

Figure 1: Crystal structures of cubic Cs_2NaScI_6 and Cs_2NaYI_6 at T = 414 K and cubic Cs_2NaScI_6 at room temperature from single-crystal X-ray diffraction studies. Grey polyhedra are around Na and blue polyhedra are around Sc or Y. Thermal ellipsoids are depicted at 50 % probability. The room-temperature structure of monoclinic Cs_2NaYI_6 was optimized (DFT-PBE-D3) based on cell parameters obtained by a Pawley fit of powder X-ray diffraction data.

Table 1: Detailed results from the structural refinements with single-crystal X-ray diffraction data and Pawley fitting of powder data in the case of $P2_1/n$ Cs_2NaYI_6. Comparisons to select structural parameters from density functional theory (DFT) calculations using the VASP suite with the PBE functional and D3 dispersion corrections are also shown. I–I distances in the last column correspond to M(III)I_6 octahedra.

Cubic Fm–$3m$						
Compound	T (K)/DFT	Cell	Cs–I (Å)	Na–I (Å)	M(III)–I (Å)	I–I (Å)
Cs_2NaScI_6	414	a = 12.02(3) Å	4.251(1)	3.145(8)	2.862(7)	4.049(1)
Cs_2NaScI_6	298	a = 11.917(5) Å	4.215(2)	3.110(2)	2.849(2)	4.029(3)
Cs_2NaScI_6	DFT	a = 11.89 Å	4.206	3.077	2.871	4.059
Cs_2NaYI_6	414	a = 12.23(2) Å	4.326(6)	3.135(5)	2.983(5)	4.218(7)
Cs_2NaYI_6	DFT	a = 12.13 Å	4.289	3.071	2.992	4.232
Monoclinic $P2_1/n$						
Cs_2NaScI_6	DFT	V = 838.3 Å^3	4.001 (avg.)	3.121 (avg.)	2.883 (avg.)	
Cs_2NaYI_6	298	V = 890.41(2) Å^3				
Cs_2NaYI_6	DFT	V = 881.1 Å^3	4.000 (avg.)	3.137 (avg.)	3.013 (avg.)	

Table 1 presents results from the structural refinements and density functional theory (DFT) based structural relaxations using the Vienna Ab initio Simulation Package (VASP) [38, 39, 40] with the PBE functional [41] and D3 dispersion corrections.[42, 43] At T = 414 K, when both compounds are cubic, the M–I distances are 2.849(2) Å and 2.983(5) Å for Cs_2NaScI_6 and Cs_2NaYI_6, respectively. The Na–I distances are 3.109(2) Å and 3.135(5) Å. The Y–I (radius of 0.900 Å) [44, 45] bond distance compares well with the previously reported Dy–I distance (2.978(3) Å, Dy(III) = 0.912 Å) in Cs_2NaDyI_6, while the smaller Sc(III) cation (radius of 0.745 Å) [44, 45] has a significantly shorter Sc–I distance. The minimal thermal expansion observed in Cs_2NaScI_6 is likely due to the anisotropic displacement parameters of iodine, which favor transverse vibrational modes. [46] At the limit of octahedral stability (μ = 0.414), we expect the I–I distances to be 4.40 Å, or twice the radius of iodide. In the room temperature Cs_2NaScI_6 structure, the I–I distance for the Na octahedra matches this value almost exactly, which is unsurprising given the radius ratio of μ = 0.46. The I–I distance for the Sc octahedra, however, deviates significantly with a value of 4.03 Å. This discrepancy suggests that the increased covalency associated with the smaller Sc(III) cation leads to shorter M–I distances. [47] We note that there have been recent suggestions of revised ionic radii to more reliably deal with the crystallography of halides,[48] but it appears that the usual Shannon[44, 45] radii can explain the observed trends in this work.

Differential scanning calorimetry measurements (DSC) indicate that Cs_2NaScI_6 undergoes a structural transition at T = 222 K, whereas Cs_2NaYI_6 undergoes a transition close to T = 395 K. The DSC data is plotted and presented in the Supporting Information. These findings align with the general trend observed for iodide double perovskites, where compounds with smaller trivalent cations undergo this structural transition at lower temperatures. [22] The predictive factors for double perovskite formation are the adapted tolerance factor [29]:

$$t' = (r_{Cs} + r_I)/[\sqrt{2} \times ((r_{Na} + r_M)/2 + r_I)]$$

and the radius ratio m = r_M/r_I. These shed light on stability and the compositional dependence of the structural transition temperature. Double perovskites are expected to be cubic for 0.88< t' < 1.00 [29], although it has been noted that this range may deviate slightly depending on the halide in question.[49]

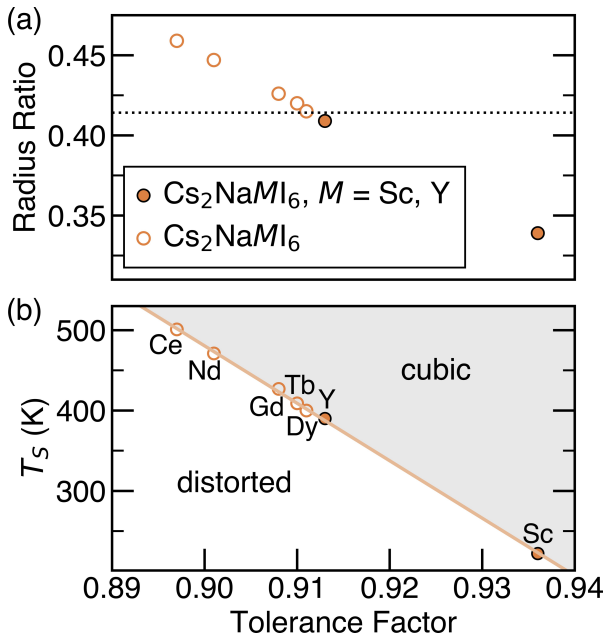

Figure 2: (a) Stability field displaying the location of the iodide double perovskites reported here and previously [22] in the space of the tolerance factor t' and the octahedral factor m. The dashed horizontal line at indicates the expected lower limit of stability. (b) Transition temperatures from cubic to lower symmetry as determined by scanning calorimetry for the different iodide double perovskites.

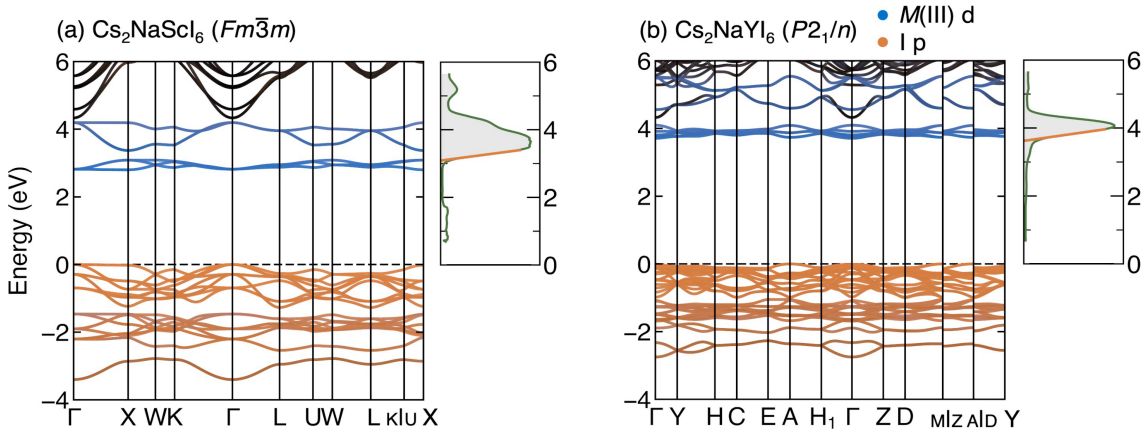

Figure 3: Band structures with Kubelka-Munk–transformed optical absorption spectra plotted alongside for (a) Cs_2NaScI_6 and (b) Cs_2NaYI_6. The band structures were calculated for the room-temperature structures ($Fm\bar{3}m$ for Cs_2NaScI_6 and $P2_1/n$ for Cs_2NaYI_6) using DFT-PBE-D3 with the Δ-sol correction applied as a scissor. Solid orange lines in the optical spectra correspond to analysis of absorption onset for direct band gap systems.

Figure 2 illustrates these predictive factors alongside the structural transition temperatures for various $Cs_2Na\mathit{M}I_6$ compositions, where M = Sc, Y, Ce, Nd, Er, Gd, Dy. Figure 2(a) plots the radius ratio against the tolerance factor. The dotted horizontal line represents the minimum value predicted for octahedral coordination. It is evident that Sc(III) is notably undersized for this coordination environment with iodide, whereas Y(III) approaches the threshold of size compatibility. The smaller size of the Sc cation likely accounts for why Cs_2NaScI_6 maintains a cubic structure at room temperature. Figure 2(b) shows the observed trend for the structural transition temperature and suggests that the range for obtaining cubic iodide double perovskites at room temperature is more stringent than expected. Raman spectra for Cs_2NaScI_6 and Cs_2NaYI_6 were also acquired and are presented and explained in the Supporting Information. Density functional theory (DFT) calculations were carried out to better understand the electronic structure of these materials and elucidate the results seen above. Figure 3(a) and (b) shows the PBE-D3 band structures with the Δ-sol correction [50] for Cs_2NaScI_6 and Cs_2NaYI_6 in their respective room-temperature phases, cubic and monoclinic. The band structure for the monoclinic $P2_1/n$ Cs_2NaYI_6 phase was calculated starting with the room-temperature unit cell parameters determined from the Pawley fit to the powder X-ray diffraction data (Supporting Information) and atomic positions from the isostructural room-temperature structure of Cs_2NaCeI_6. The Δ-sol calculated band gap energies are 2.80 eV for Cs_2NaScI_6 and 3.52 eV ($Fm\bar{3}m$) and 3.71 eV ($P2_1/n$) for Cs_2NaYI_6.

All calculated band structures show a direct band gap with relatively little conduction band dispersion. The small dispersion is expected given the interruption of M(III)–I bonding by ionic Na^+. Furthermore, the orbital projections in the band structures show no contribution from the Na(I) cation at the conduction band minimum and only M(III)–I participation. The slightly

larger band gap for monoclinic Cs_2NaYI_6 compared to cubic Cs_2NaScI_6 is expected given the lower symmetry. The ≈0.7 eV difference between the band gap energies of Cs_2NaScI_6 and cubic Cs_2NaYI_6 can be accounted for by the increased iodide dispersion in the smaller Cs_2NaScI_6.

Solid-state diffuse reflectance spectra are also shown in Figure 3 for Cs_2NaScI_6 and Cs_2NaYI_6 alongside the band structures. Data were collected and transformed to normalized absorbance by the Kubelka-Munk function. The absorbances for Cs_2NaScI_6 and Cs_2NaYI_6 are centered at 3.25 eV and 4.03 eV, respectively and are assigned to a ligand-to-metal charge transfer (LMCT) between the iodide to either Sc(III) or Y(III). The higher energy LMCT for Cs_2NaYI_6 is expected given the longer *M*(III)–I distances.[51] The band gaps (or, more accurately, the optical absorption edges) were obtained using the the usual relation for a direct band gap semiconductor.[52] Fitting the rising linear region of the LMCT shows that the optical absorption edge energies occur at approximately 3.10 eV and 3.65 eV for Cs_2NaScI_6 and Cs_2NaYI_6, respectively. The analogous Cs_2Na*M*I_6 (*M* = Ce, Nd, Gd, Tb, Dy) optical absorption edge energies occur between 3.3 eV to 3.4 eV and are also similar in shape.[22] It is seen from Figure 3 that the PBE-D3-Δ-sol calculations are effective in capturing the experimental band gaps, and also the absorption dip beyond the initial manifold of empty d states of Sc or Y.

As mentioned previously, the competing phase that forms during the synthesis for the Sc system is the 3:2:9 compound $Cs_3Sc_2I_9$, for which we were able to obtain single crystals and a reliable structure solution. The crystal structure of the $Cs_3Sc_2I_9$ phase is of the $Cs_3Cr_2Cl_9$ structure-type (details in Supporting Information).

To better understand the energetic competition between iodide double perovskites and the competing 3:2:9 compounds, we carried out first-principles DFT calculations associated with the decomposition reaction:

$$2\,Cs_2Na\mathit{M}I_6 \rightarrow Cs_3\mathit{M}_2I_9 + 2NaI + CsI \qquad (2)$$

in a manner similar to what has been employed by Savory *et al.* [53] for other related compounds. The 3:2:9 structure type involving face-shared M_2I_9 polyhedra — the $Cs_3Cr_2Cl_9$ structure type — was used in all cases. The data are displayed in Table 2 and include cations beyond Sc(III) and Y(III). We find that while Cs_2NaYI_6 is expected to be stable as a double perovskite, Cs_2NaScI_6 is metastable, which aligns with our frequent observation of $Cs_3Sc_2I_9$ crystals in the reaction products. While In(III) and Sb(III) are larger than Sc(III), they do not appear to form stable iodide double perovskites. Similarly,

Table 2: DFT-PBE-D3 energetics of the decomposition reaction to a 3:2:9 phase $Cs_3M(III)_2I_9$ as shown in Equation 1 for *M*(III) = Sc, In, Sb, Y, La, and Bi. All structures were fully relaxed, and the monoclinic $P2_1/n$ structures were employed for the double perovskites. Details in Supporting Information.

M(III)	Energy (eV)
Sc	−0.29
In	−0.41
Sb	−0.41
Y	0.05
La	0.40
Bi	−0.32

$Cs_2M(I)BiI_6$ has been challenging to synthesize, despite having a tolerance factor and radius ratio within the limits of stability. The few reports of Bi iodide double perovskite compounds often provide limited structural information, note difficulties during synthesis, or observe fast conversion to a 3:2:9 phase. [54, 55, 56, 57, 58] Notably, many of the compounds that do not form have s^2 lone pairs that may stabilize or destabilize structures for reasons beyond simple size considerations. For example, these p-block *M*(III) cations are expected to form more covalent *M*–I bonds, thereby reducing the electrostatic I–I repulsion and enhancing the I–I van der Waals interactions. We have been able to crystallize compounds with the largest rare-earth, La, which is expected based on considerations of μ and t', as well as the DFT stability analysis. Our research also suggests the existence Cs_2NaUI_6 from powder diffraction. Accurate crystal structure determination based on single-crystal X-ray analysis for these compounds have not been possible at this time. Collectively, our results suggest that among known inorganic trivalent ions, there is not an upper size limit for stabilizing iodide double perovskites.

Conclusions

In closing, we have presented the first complete structural characterization of an iodide double perovskite that is cubic at room temperature, and some related compounds. We have shown that some iodide double perovskites form even when they contain trivalent ions that are considered too small for this structure type. DFT comparisons of enthalpies of formation have provided an explanation regarding why iodide double perovskites that would be expected to exist based on size and tolerance considerations have eluded experimental verification.

Methods

Synthesis

The double perovskite compounds were prepared by solid-state reaction of the appropriate starting materials acquired from Thermo Scientific (ScI_3: 99.999%, YI_3: 99.9%, CsI: 99.998% and NaI: 99.999%). MI_3 with 2 equivalents of CsI and 1 equivalent of NaI at 675 °C in an alumina crucible placed in a sealed and evacuated silica tube, with all reactant and sample manipulation under strictly air-free and anhydrous conditions (Supporting Information). Directly quenching the reaction tube into water after removal from the furnace yielded the cleanest samples. In order to remove any persistent oxygen-containing impurities, the compounds were purified through a self-flux/transport method (details in SI). This method affords high purity, crystalline materials that are free of any oxygen or binary salt-containing impurities, noting that these compounds are extremely sensitive to moisture and decompose instantly upon exposure to ambient air. The reaction conditions for Cs_2NaScI_6 often yielded $Cs_3Sc_2I_9$ crystals. Bulk powders of the latter were prepared using the procedure detailed above, but with 2 equivalents ScI_3 and 3 equivalents CsI.

Single-crystal X-ray diffraction

Single-crystal X-ray diffraction data for Cs_2NaMI_6 (M = Sc, Y) and $Cs_3Sc_2I_9$ were collected on a Bruker KAPPA APEX II diffractometer equipped with an APEX II CCD detector, a TRIUMPH monochromator, and a Mo-Kα radiation source (λ = 0.71073 A). Crystals° were mounted on a quartz rod under Paratone-N oil, and data were collected at 298(2) K for Cs_2NaScI_6 and $Cs_3Sc_2I_9$ and at 414(2) K for $Cs_2Na$$MI_6$ (M = Sc, Y) using an Oxford nitrogen gas cryostream system. Data collection and cell parameter determination were conducted using the SMART program.[59] Structure solution and refinement were performed using SHELXTL.[60] All crystal structures are visualized using the VESTA software package.[61] Further crystallographic details can be found in the Supporting Information.

Powder diffraction

Powder X-ray diffraction (PXRD) measurements were performed on a Panalytical Empyrean powder diffractometer in reflection mode with a Cu-Kα radiation source with the samples placed in a air-free holder with Be windows. The data were analyzed using the TOPAS software suite[62] and Pawley refinements[63] were performed to determine lattice parameters and peak shapes.

Differential Scanning Calorimetry

Differential Scanning Calorimetry (DSC) was performed using a TA Instruments DSC Q2000 at a heating/cooling rate of 10 °Cmin^{-1} using between 3 and 5 mg of sample in a sealed aluminum pan.

UV-Vis spectroscopy

Diffuse reflectance UV-Vis spectra were collected on a Shimadzu UV-3600 UV–vis–NIR spectrometer equipped with an integrating sphere. $BaSO_4$ (Sigma Aldrich) was used as the reference for 100% reflectance. Samples were diluted with $BaSO_4$ and loaded in the sample holder inside the glovebox. Transparent tape was placed over the samples to limit decomposition from exposure to air. The diffuse reflectance data were converted to absorbance using the Kubelka-Munk transformation.[64]

Raman Spectroscopy

Raman spectroscopy and photoluminescence measurements were performed at room temperature using a Horiba Jobin Yvon T64000 open-frame confocal microscope operating at a wavelength of 488nm with triple monochromator and LN_2-cooled CCD array detector. Due to the air-sensitivity of the samples, the powders were loaded into a homemade air-free cell with a fused silica window (Corning glass) inside a glovebox. Spectra were calibrated by referencing the monocrystalline silicon peak at $521cm^{-1}$. The spectrum of silicon inside the air-free cell was used to confirm that the use of the cell only contributes very minor peaks or changes to the baseline.

Electronic structure calculations

Electronic structure calculations were performed using density functional theory (DFT) as implemented in the Vienna Ab initio Simulation Package v5.4.4. [38,39,40] The calculations used the VASP-recommended projector-augmented wave potentials and Perdew-Burke-Ernzerhof (PBE)[41] functionals with D3 corrections using Becke-Johnson damping (IVDW = 12)[42,43] were additionally employed because of the presence of large and polarizable ions such as Cs^+ and I^-. An energy convergence better than 10^{-6} eV was employed for all calculations, with a plane-wave energy cut-off of 500 eV. Automatic *k*-mesh generation was used with the length parameter *l* set to 50. Complete structural parameters from single crystal diffraction, or cell parameters from Pawley fits of powder X-ray diffraction were employed as starting structures and all crystal structures were fully relaxed. Band structure calculations were performed using a density of 30 *k*-points *per* branch with an AFLOW generated k-point path.[65] The Δ-sol correction method, as detailed by Chan and Ceder,[50] was used to compensate for the usual PBE underestimation of band gaps. For the relative phase stability calculations, all double perovskite energies are taken from the fully relaxed monoclinic structures. The energies of the 3:2:9 phases use the fully relaxed $Cs_3Cr_2Cl_9$-type structures, which are the most stable for all the relevant 3:2:9 compositions.

Supporting Information Summary:

Supporting information containing table of crystallographic data and other characterization (powder X-ray diffraction, Raman spectroscopy, and DSC).

Deposition Number(s) <url href="https://www.ccdc.cam.ac.uk/services/structures?id=doi:10.1002/chem.202404009">2378641 (Cs2NaScI6-298K), 2378642 (Cs2NaScI6-414K), 2378643 (Cs2NaYI6-414K), 2378644 (Cs2NaYI6-298K)</url> contain(s) the supplementary crystallographic data for this paper. These data are provided free of charge by the joint Cambridge Crystallographic Data Centre and Fachinformationszentrum Karlsruhe <url href="http://www.ccdc.cam.ac.uk/structures">Access Structures service</url>.

Acknowledgements

This work was supported by the U. S. Department of Energy, Office of Science, Basic Energy Sciences, under DE-SC0024422, and made use of shared facilities of the National Science Foundation (NSF) Materials Research Science and Engineering Center (MRSEC) at UC Santa Barbara (NSF DMR 2308708). A.K.C. thanks the Ras al Khaimah Centre for Advanced Materials for financial support. Use was made of computational facilities purchased with support from the National Science Foundation (CNS-1725797) and administered by the Center for Scientific Computing (CSC). The CSC is supported by the California NanoSystems Institute and the Materials Research Science and Engineering Center (MRSEC; NSF DMR 2308708) at UC Santa Barbara.

Conflict of Interest

None.

Data Availability Statement:

Data associated with this publication is available from the authors on reasonable request.

References

[1] N. R. Wolf, B. A. Connor, A. H. Slavney, H. I. Karunadasa, *Angew. Chem. Int. Ed.* **2021**, *60*, 16264.
[2] A. Kojima, K. Teshima, Y. Shirai, T. Miyasaka, *J. Am. Chem. Soc.* **2009**, *131*, 6050.
[3] J.-H. Im, C.-R. Lee, J.-W. Lee, S.-W. Park, N.-G. Park, *Nanoscale* **2011**, *3*, 4088.
[4] H.-S. Kim, C.-R. Lee, J.-H. Im, K.-B. Lee, T. Moehl, A. Marchioro, S.-J. Moon, R. Humphry-Baker, J.-H. Yum, J. E. Moser, et al., *Sci. Rep.* **2012**, *2*, 591.
[5] I. Chung, B. Lee, J. He, R. P. Chang, M. G. Kanatzidis, *Nature* **2012**, *485*, 486.
[6] M. M. Lee, J. Teuscher, T. Miyasaka, T. N. Murakami, H. J. Snaith, *Science* **2012**, *338*, 643.
[7] N. Pellet, P. Gao, G. Gregori, T.-Y. Yang, M. K. Nazeeruddin, J. Maier, M. Grätzel, *Angew. Chem. Int. Ed.* **2014**, *53*, 3151.
[8] B. V. Lotsch, *Angew. Chem. Int. Ed.* **2014**, *53*, 635.
[9] F. Giustino, H. J. Snaith, *ACS Energy Lett.* **2016**, *1*, 1233.
[10] S. Gupta, T. Bendikov, G. Hodes, D. Cahen, *ACS Energy Lett.* **2016**, *1*, 1028.
[11] W. Ning, F. Gao, *Adv. Mater.* **2019**, *31*, 1900326.
[12] P. Vishnoi, J. Zuo, T. A. Strom, G. Wu, S. D. Wilson, R. Seshadri, A. K. Cheetham, *Angew. Chem.* **2020**, *59*, 8974.
[13] A. J. Lehner, H. Wang, D. H. Fabini, C. D. Liman, C.-A. He´bert, E. E. Perry, M. Wang, G. C. Bazan, M. L. Chabinyc, R. Seshadri, *Appl. Phys. Lett.* **2015**,*107*, 131109.
[14] A. H. Slavney, T. Hu, A. M. Lindenberg, H. I. Karunadasa, *J. Am. Chem. Soc.* **2016**, *138*, 2138.
[15] E. T. McClure, M. R. Ball, W. Windl, P. M. Woodward, *Chem. Mater.* **2016**, *28*, 1348.
[16] Z. Zhang, Y. Liang, H. Huang, X. Liu, Q. Li, L. Chen, D. Xu, *Angew. Chem. Int. Ed.* **2019**, *58*, 7263.
[17] K. T. Kluherz, S. T. Mergelsberg, J. J. De Yoreo, D. R. Gamelin, *Chem. Mater.* **2023**, *35*, 5699.
[18] F. Wei, Z. Deng, S. Sun, F. Zhang, D. M. Evans, G. Kieslich, S. Tominaka, M. A. Carpenter, J. Zhang, P. D. Bristowe, et al., *Chem. Mater.* **2017**, *29*, 1089.
[19] H. J. Snaith, *J. Phys. Chem. Lett.* **2013**, *4*, 3623.
[20] P. Yang, F. P. Doty, M. A. Rodriguez, M. R. Sanchez, X. Zhou, K. S. Shah, *MRS Proc.* **2009**, *1164*, 1164.
[21] G. Gundiah, K. Brennan, Z. Yan, E. Samulon, G. Wu, G. Bizarri, S. Derenzo, E. Bourret-Courchesne, *J. Lumin.* **2014**, *149*, 374.
[22] G. T. Kent, E. Morgan, K. R. Albanese, A. Kallistova, A. Brumberg, L. Kautzsch, G. Wu, P. Vishnoi, R. Seshadri, A. K. Cheetham, *Angew. Chem.* **2023**, *135*, e202306000.
[23] B. Vargas, G. Rodrıguez-López, D. Solis-Ibarra, *ACS Energy Lett.* **2020**, *5*, 3591.
[24] H. A. Evans, L. Mao, R. Seshadri, A. K. Cheetham, *Annu. Rev. Mater. Res.* **2021**, *51*, 351.
[25] M. S. Lassoued, T. Wang, A. Faizan, Q.-W. Li, W.-P. Chen, Y.-Z. Zheng, *J. Mater. Chem. C* **2022**, *10*, 12574.
[26] M. S. Lassoued, T. Wang, Q.-W. Li, X. Liu, W.-P. Chen, B. Jiao, Q.-Y. Yang, Z. Wu, G. Zhou, S. Ding, et al., *Mater. Chem. Frontiers* **2022**, *6*, 2135.
[27] Q.-W. Li, L.-Y. Bi, M. S. Lassoued, Q.-C. Luo, R. Yan, X.-K. Ding, G.-Y. Gou, Y.-Z. Zheng,

Nanoscale **2023**, *15*, 5265.
[28] P. Vishnoi, R. Seshadri, A. K. Cheetham, *J. Phys. Chem. C* **2021**, *125*, 11756.
[29] D. Babel, R. Haegele, G. Pausewang, F. Wall, *Mater. Res. Bull.* **1973**, *8*, 1371.
[30] W. B. Jensen, W. B. Jensen, *J. Chem. Educ.* **2010**, *87*, 3387.
[31] D. Guthrie, G. Meyer, J. Corbett, *Inorg. Chem.* **1981**, *20*, 1192.
[32] M. Lenck, A. Weiss, *Z. Naturforsch. A* **1992**, *47*, 54.
[33] K. M. McCall, C. C. Stoumpos, S. S. Kostina, M. G. Kanatzidis, B. W. Wessels, *Chem. Mater.* **2017**, *29*, 4129.
[34] A. J. Lehner, D. H. Fabini, H. A. Evans, C.-A. He´bert, S. R. Smock, J. Hu, H. Wang, J. W. Zwanziger, M. L. Chabinyc, R. Seshadri, *Chem. Mater.* **2015**, *27*, 7137.
[35] Z. Deng, F. Wei, Y. Wu, R. Seshadri, A. K. Cheetham, P. Canepa, *Inorg. Chem.* **2020**, *59*, 3377.
[36] G. Meyer, *Z. Naturforsch. B* **1980**, *35*, 394.
[37] G. Meyer, J. D. Corbett, *Inorg. Chem.* **1981**, *20*, 2627.
[38] G. Kresse, J. Hafner, *Phys. Rev. B* **1994**, *49*, 14251.
[39] G. Kresse, J. Furthmüller, *Comput. Mater. Sci.* **1996**, *6*, 15.
[40] G. Kresse, D. Joubert, *Phys. Rev. B* **1999**, *59*, 1758.
[41] J. P. Perdew, K. Burke, M. Ernzerhof, *Phys. Rev. Lett.* **1996**, *77*, 3865.
[42] S. Grimme, J. Antony, S. Ehrlich, H. Krieg, *J. Chem. Phys.* **2010**, *132*, 154104.
[43] S. Grimme, S. Ehrlich, L. Goerigk, *J. Comput. Chem.* **2011**, *32*, 1456.
[44] R. D. Shannon, C. T. Prewitt, *Acta Crystallogr. B* **1969**, *25*, 925.
[45] R. D. Shannon, *Acta Crystallogr. B* **1976**, *32*, 751.
[46] H. D. Megaw, *Mater. Res. Bull.* **1971**, *6*, 1007.
[47] F. A. Cotton, G. Wilkinson, C. A. Murillo, M. Bochmann, *Advanced Inorganic Chemistry*, John Wiley & Sons **1999**.
[48] W. Travis, E. Glover, H. Bronstein, D. Scanlon, R. Palgrave, *Chem. Sci.* **2016**, *7*, 4548.
[49] I. Flerov, M. Gorev, K. Aleksandrov, A. Tressaud, J. Grannec, M. Couzi, *Mater. Sci. Eng. R Rep.* **1998**, *24*, 81.
[50] M. K. Chan, G. Ceder, *Phys. Rev. Lett.* **2010**, *105*, 196403.
[51] P. Vishnoi, J. L. Zuo, J. A. Cooley, L. Kautzsch, A. Gómez-Torres, J. Murillo, S. Fortier, S. D. Wilson, R. Seshadri, A. K. Cheetham, *Angew. Chem.* **2021**, *133*, 5244.
[52] A. Dolgonos, T. O. Mason, K. R. Poeppelmeier, *J. Solid State Chem.* **2016**, *240*, 43.
[53] C. N. Savory, A. Walsh, D. O. Scanlon, *ACS Energy Lett.* **2016**, *1*, 949.
[54] S. E. Creutz, E. N. Crites, M. C. De Siena, D. R. Gamelin, *Nano Lett.* **2018**, *18*, 1118.
[55] C. Zhang, L. Gao, S. Teo, Z. Guo, Z. Xu, S. Zhao, T. Ma, *Sustain. Energy Fuels* **2018**, *2*, 2419.
[56] P. Li, W. Gao, C. Ran, H. Dong, X. Hou, Z. Wu, *Phys. Status Solidi A* **2019**, *216*, 1900567.
[57] L. Peedikakkandy, S. Chatterjee, A. J. Pal, *J. Phys. Chem. C* **2020**, *124*, 10878.
[58] Y. Zheng, F. Luo, L. Ruan, J. Tong, L. Yan, C. Sun, X. Zhang, *J. Alloys Compd.* **2022**, *909*, 164613.
[59] Bruker AXS Inc., SMART, Apex II, Version 2.1, Madison, WI 2005.
[60] Bruker AXS Inc., SHELXTL PC, Version 6.12 Ed., Madison, WI 2005.
[61] K. Momma, F. Izumi, J. Appl. Crystallogr. 2011, 44, 1272.

[62] A. A. Coelho, J. Appl. Crystallogr. 2018, 51, 210.
[63] G. S. Pawley, J. Appl. Crystallogr. 1981, 14, 357.
[64] P. Kubelka, Z. Phys. 1931, 12, 593.
[65] S. Curtarolo, W. Setyawan, G. L. Hart, M. Jahnatek, R. V. Chepulskii, R. H. Taylor, S. Wang, J. Xue, K. Yang, O. Levy, M. J. Mehl, H. T. Stokes, D. O. Demchenko, D. Morgan, Computational Mater. Sci. 2012, 58, 218.

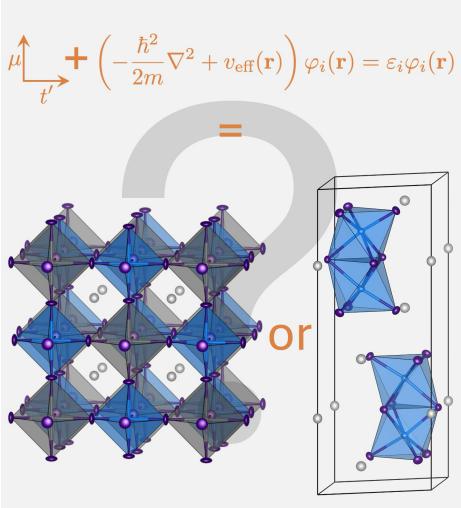

What determines the stability of iodide double perovskites and our ability to synthesize them? Despite being highly sought after, not a lot is known about this rare compositional family. We present the single crystal X-ray structures of two iodide double perovskites containing small trivalent ions, and employ design rules for perovskites, coupled with electronic structure calculations, to understand stability limits.

Supporting Information for:

Iodide Double Perovskites and the Limits of their Structural Stability

Anya S. Mulligan,[+,a] Greggory T. Kent,[+,a] Jiale Zhuang,[a]
Arava Zohar,[a] Kaitlin R. Albanese,[a] Emily E. Morgan,[a]
Guang Wu,[+,b] Anthony K. Cheetham,*[c] Ram Seshadri*[d]

[a] Anya S. Mulligan, Dr. Greggory T. Kent, Jiale Zhuang, Dr. Kaitlin R. Albanese, Dr. Emily E. Morgan, Dr. Arava Zohar
Materials Department and Materials Research Laboratory
University of California, Santa Barbara, California 93106, United States

[b] Dr. Guang Wu
Department of Chemistry and Biochemistry
University of California, Santa Barbara, California 93106, United States

[c] Professor Sir Anthony K. Cheetham
Materials Department and Materials Research Laboratory
University of California, Santa Barbara, California 93106, United States
Department of Materials Science and Engineering
National University of Singapore, Singapore 117575, Singapore
Email: akc30@cam.ac.uk

[c] Professor Ram Seshadri
Materials Department and Materials Research Laboratory
Department of Chemistry and Biochemistry
University of California, Santa Barbara, California 93106, United States
Email: seshadri@mrl.ucsb.edu

[+] These authors contributed equally.

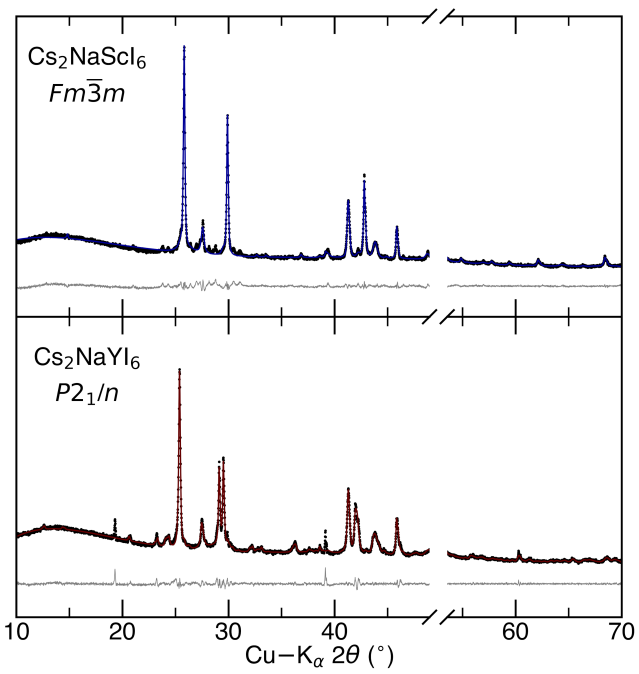

Figure S 1: Pawley fits to the room temperature X-ray powder diffraction data of Cs_2NaScI_6 and Cs_2NaYI_6 respectively in the $Fm\bar{3}m$ and $P2_1/n$ space groups.

Results

The cubic double perovskite structure is predicted to have four Raman active modes, three internal modes and one lattice mode.[1, 2, 3] The MI_6^{-3} octahedra in double perovskites possess O_h symmetry, leading to three primary internal Raman active modes: ν_1 (A_{1g}), ν_2 (E_g), and ν_5 (T_{2g}).[4, 5] ν_1 is the symmetric stretching mode, ν_2 the asymmetric stretching mode, and ν_5 the bending mode of the MI_6^{-3} octahedron. Additionally, the cubic double perovskite structure features a translational lattice mode which is also Raman active, classified as T_{2g}. [4] In the Cs_2NaScI_6, Raman spectroscopy reveals a peak at 69 cm^{-1} corresponding to ν_5 (T_{2g}), a peak at 112 cm^{-1} corresponding to ν_2 (Eg), and a peak at 132 cm^{-1} corresponding to ν_1 (A_{1g}). These frequencies generally satisfy the relation ${\nu_1}^2 \approx {\nu_2}^2 + \frac{3}{5}{\nu_5}^2$.[1, 4] We attribute the small peak at 171 cm^{-1} to residual I_2 in the sample[6] and the peak at 93 cm^{-1} is potentially from residual CsI.[7]

For Cs_2NaYI_6 in the monoclinic $P2_1/n$ room temperature structure, we expect 24 Raman active modes: 12 A_g and 12 B_g modes. The absence of some of these peaks can likely be explained by modes occurring at the same frequencies or being too low intensity to be observable. Based on the frequencies observed in the chloride analogs of these iodide double perovskites [8, 9] and similar bromide compositions [10], the T_{2g} lattice modes are expected to be of too-low frequency to be observed in these spectra.

Table S1: Lattice parameters determined from Pawley fits.

Formula	Cs_2NaScI_6	Cs_2NaYI_6
Crystal System	Cubic	Monoclinic
Space Group	$Fm\bar{3}m$	$P2_1/n$
Cell Volume (Å^3)	1704.6(2)	890.41(2)
a (Å)	11.938(6)	8.5026(4)
b (Å)	11.938(6)	8.5488(3)
c (Å)	11.938(6)	12.250(6)
α	90	90
β (°)	90	90.284(2)
γ (°)	90	90
R_{wp}	4.75%	3.68%
R_p	3.49%	2.61%

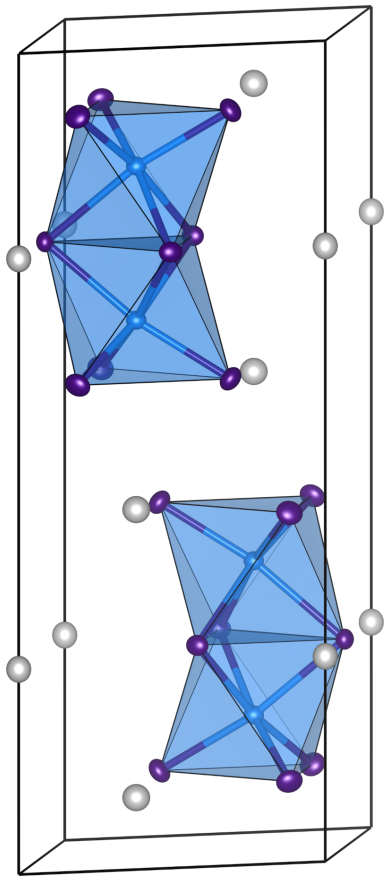

Figure S 2: $Cs_3Sc_2I_9$ single crystal structure at room temperature displaying atomic displacement parameters with 50 % probability.

Table S2: Details of the single-crystal X-ray diffraction measurements.

Structure	Cs_2NaScI_6-298K	Cs_2NaScI_6-414K	Cs_2NaYI_6-414K	$Cs_3Sc_2I_9$-298K
CCDC/FIZ deposition #	2378641	2378642	2378643	2378644
T (K)	298(2)	414(2)	414(2)	298(2)
Crystal Habit, Color	Plate, Colorless	Plate, Colorless	Plate, Colorless	Block, Colorless
Crystal Size (mm)	0.15×0.15×0.05	0.15×0.15×0.05	0.15×0.10××0.05	0.30×0.30×0.20
Crystal System	Cubic	Cubic	Cubic	Hexagonal
Space Group	$Fm\bar{3}m$	$Fm\bar{3}m$	$Fm\bar{3}m$	$P6_3/mmc$
Cell Volume (Å^3)	1693(2)	1735(1)	1831(1)	1214(3)
a (Å)	11.917(5)	12.02(3)	12.234(2)	8.250(9)
b (Å)	11.917(5)	12.02(3)	12.234(2)	8.250(9)
c (Å)	11.917(5)	12.02(3)	12.234(2)	20.60(2)
α (○)	90	90	90	90
β (○)	90	90	90	90
γ (○)	90	90	90	120
Z	4	4	4	2
FW (g mol^{-1})	1095.17	1095.17	1139.12	1630.75
Calc. Density (g cm$^-3$)	4.298	4.193	4.132	4.461
Abs. Coeff. (mm^{-1})	15.601	15.221	17.203	16.414
F_{000}	1840	1840	1912	1368
Total No. Reflections	943	618	505	2589
Unique Reflections	125	122	136	621
R_{int}	0.0372	0.0655	0.0399	0.0350
Final R Indices	R_1 = 0.0333	R_1 = 0.0618	R_1 = 0.0368	R_1 = 0.0306
$[I > 2\sigma(I)]$	wR_2 = 0.0731	wR_2 = 0.1296	wR_2 = 0.1161	wR_2 = 0.0719
Largest Δ (e Å$^-3$)	0.825 and −0.543	0.978 and −1.430	0.590 and −0.699	1.107 and −0.838
GOF	1.145	1.087	1.093	1.147

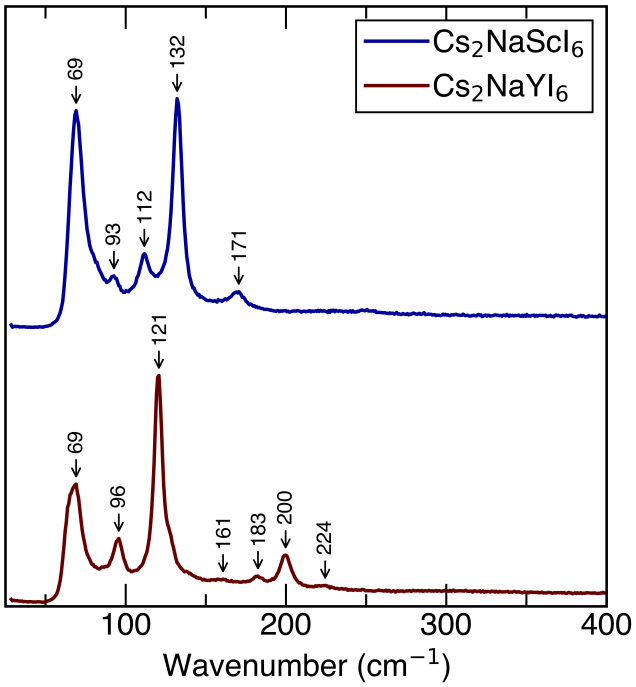

Figure S 3: Raman spectra for Cs_2NaScI_6 and Cs_2NaYI_6 at room temperature.

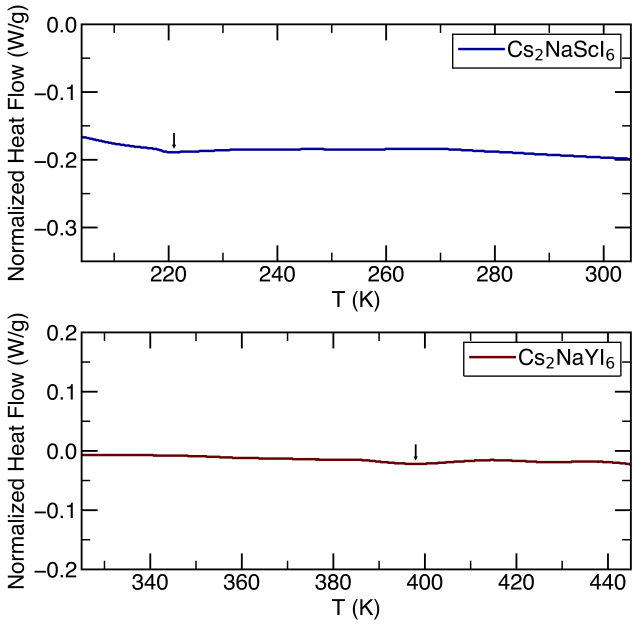

Figure S 4: DSC traces for Cs_2NaScI_6 and Cs_2NaYI_6

References

[1] D. M. Yost, C. C. Steffens, S. T. Gross, *J. Chem. Phys.* **1934**, *2*, 311.

[2] G. Papatheodorou, *Inorg. Nucl. Chem. Lett.* **1975**, *11*, 483.

[3] M. Couzi, S. Khairoun, A. Tressaud, *phys. status solidi a* **1986**, *98*, 423.

[4] G. Papatheodorou, *J. Chem. Phys.* **1977**, *66*, 2893.

[5] E. Hahn, R. Hebisch, *Spectrochim. Acta A* **1991**, *47*, 1097.

[6] A. Anderson, T. Sun, *Chem. Phys. Lett.* **1970**, *6*, 611.

[7] M. Metallinou, L. Nalbandian, G. Papatheodorou, W. Voigt, H. Emons, *Inorg. Chem.* **1991**, *30*, 4260.

[8] W. Smit, G. Dirksen, D. Stufkens, *J. Phys. Chem. Solids* **1990**, *51*, 189.

[9] G. Zissi, G. Papatheodorou, *Chem. Phys. Lett.* **1999**, *308*, 51.

[10] G. Photiadis, B. Brresen, G. Papatheodorou, *J. Chem. Soc. Faraday Trans.* **1998**, *94*, 2605.